Interfacial Energies in Nanocrystalline Complex Oxides

Ricardo H. R. Castro

Department of Materials Science and Engineering, University of California-Davis, CA 95616, USA

Abstract

This paper presents a brief description of the role of interfacial energies in the understanding and control of nanocrystalline complex oxides in both particulate and bulk forms. Interfacial energies are fundamental parameters in microstructural evolution processes such as phase transformation, grain growth, and sintering. Although generally considered constant driving forces, experimental evidences confirm the possibility of intentional modification of both surface and grain boundary energies in oxide systems via ionic doping. This opened the perspective for a systematic understanding of their roles as refining parameters in microstructural control during processing and in operation. In this work we introduce the theoretical framework in the context of Gibbs adsorption isotherm and the formation of dopant excess (i.e. interfacial solute segregation) in a similar manner as formalized for liquid systems. We then present a collection of data demonstrating interfacial energy control in oxides and discuss the microstructural relationships highlighting specific examples. The data advocates for a paradigm shift on nanocrystalline processing control from a traditionally kinetically oriented perspective to a more balanced viewpoint in which thermodynamics can play a governing role, especially at moderate temperatures. The work is not an extensive review, but rather has the goal of introducing the reader to this growing research topic.

1. Introduction.

Fundamental properties of materials change at the nanoscale not only because of the reduced dimensions, but also because a large fraction of the atoms are located at the interfacial regions. This implies interfacial properties can dictate behavior, leading to unprecedented properties. While such nanoscale effects are not necessarily positive, for instance when resulting in increased solubility of complex oxides used in battery cathodes, a number of examples have demonstrated the positive impacts of having enlarged interfacial areas [1]. This improvement seems to be limited to specific interfacial properties (which sometimes are found by chance) rather than quantity alone, and when those interfaces are 'just right', they can result in improved radiation amorphisation tolerance [2, 3], unique polymorphisms [4, 5], significantly increased catalytic [6] and photoelectrocatalytic [7] activities, enhanced mechanical and ionic properties [8-11], among other benefits.

Controlling interfacial properties is certainly not a trivial task, but one can look at this problem from a thermodynamic perspective, first considering how interfacial thermodynamic states affect the material. The description of the thermodynamics of nanocrystals must of course include interfacial terms [12], which can be generally divided into two contributions: surface (solid-vapor) and grain boundaries (solid-solid). The surface term is more commonly accepted as a relevant term for particle stabilization and processing, while the grain boundaries only more recently have been demonstrated to play a major role in nanocrystals' stability against coarsening and defining polymorphism [4, 13-16]. The greatest difficulty in understanding and predicting the effect of interfacial energies in oxides has been the lack of reliable values to enable a full thermodynamic description of the system. Interfacial energies are typically small (below 1-2 $J.m^{-2}$), and therefore difficult to experimentally assess [17]. A great number of theoretical works have

been reported by Monte Carlo, DFT, and other atomistic simulations (e.g. [18-24]), but those need experimental benchmarks which in the past decade have been met by great advancements in microcalorimetry [25-27].

Although interfacial energies are indeed relatively small, at the nanoscale their energetic contributions increase as they are multiplied by the interfacial area term. For instance, in a system with surface area of $100 m^2.g^{-1}$, which is not uncommon in catalytic systems, a surface energy of 1 $J.m^{-2}$ brings an excess of $100 J.g^{-1}$. In a simple oxide such as TiO_2, this corresponds to 7.9 $kJ.mol^{-1}$, which is three times the molar free energy of phase transformation from anatase to rutile in this compound [5, 28]. In multiple examples, this affects the stable phase at a given particle size, complicating phase diagrams, as reported in the literature for aluminum oxide, Al_2O_3, for instance. Blonski and Garofalini predicted that the lower surface energy of the transitional polymorph of alumina (γ) in contrast to the corundum phase (α) would enable the existence of metastable γ-alumina in systems with high surface areas [22](**Figure 1**). This is because the total free energy of the system (bulk+surface) for γ-alumina becomes lower than for α-alumina at that critical surface area. McHale et al. experimentally demonstrated this stability cross-over by reporting experimental surface energy data for both polymorphs using high temperature oxide melt solution calorimetry [15]. The stabilization of a phase at the nanoscale because of the surface term was perhaps the first direct demonstration of the energetic differences caused by the nanoscale.

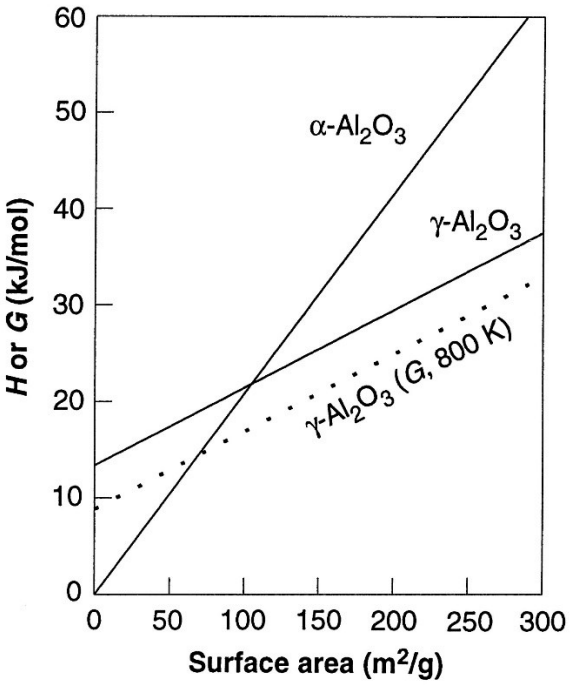

Figure 1. From Ref. 14, calculated enthalpy (H) of gamma alumina and alpha alumina relative to coarse alpha phase. The slopes represent surface energies, as reported: 2.04 $J.m^{-2}$ for α-Al_2O_3 and 0.79 Jm^{-2} for γ-Al_2O_3.

After alumina, TiO_2, ZrO_2 and iron (hydro)oxides, to cite only a few, were also reported to have polymorphism dependent on surface energies [13, 15, 29]. As one may expect, as the number of compositional elements increase, the complexity of polymorphism also does. For instance, the relative stability of *cubic*, *tetragonal, monoclinic* or *amorphous* phases in yttria-zirconia systems shows a strong dependence on both particle size (or surface area) and yttrium content [30]. **Figure 2** shows such a nanoscale phase diagram for this system, which describes the effect of particle size on the phase stability as a function of composition. The changes with relation to the respective bulk phase diagram are remarkable and show that polymorphs with the lowest surface energies (cubic and amorphous in this case) become more stable at nanoscale dimensions.

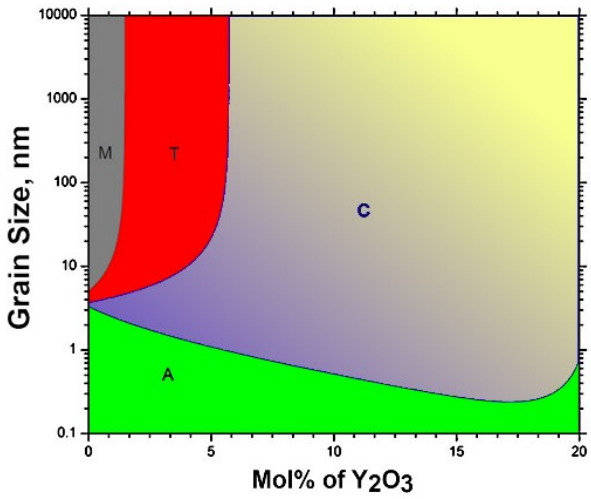

Figure 2. Phase diagram for Y_2O_3 – ZrO_2 with grain size dependence. Monoclinic polymorph stability region is indicated with (M), tetragonal polymorph with (T), cubic with (C), and the amorphous region as (A). This diagram is for room-temperature (298 K) and reproduced from Ref. 26.

Similar diagrams have been built for calcia-zirconia and scandia-zirconia [31, 32] and have meaningful practical implications, as they demonstrate, for example, the window of stability of the cubic polymorph, which is the most useful phase for the design of solid electrolytes. Although these diagrams show thermodynamic predictions fairly consistent with microstructural observations, the contribution of grain boundaries to the stability map of the polymorphs is still ignored. This shortcoming was pointed out by a work on TiO_2 proposing a more complex diagram for phase stability predictions which includes grain boundary energy as a critical term [5]. It is demonstrated that because the absolute surface energy difference between rutile and anatase TiO_2 polymorphs is not the same as their grain boundary energy differences, the fraction of surface to grain boundary area defines the stable polymorph at a given grain size (**Figure 3**).

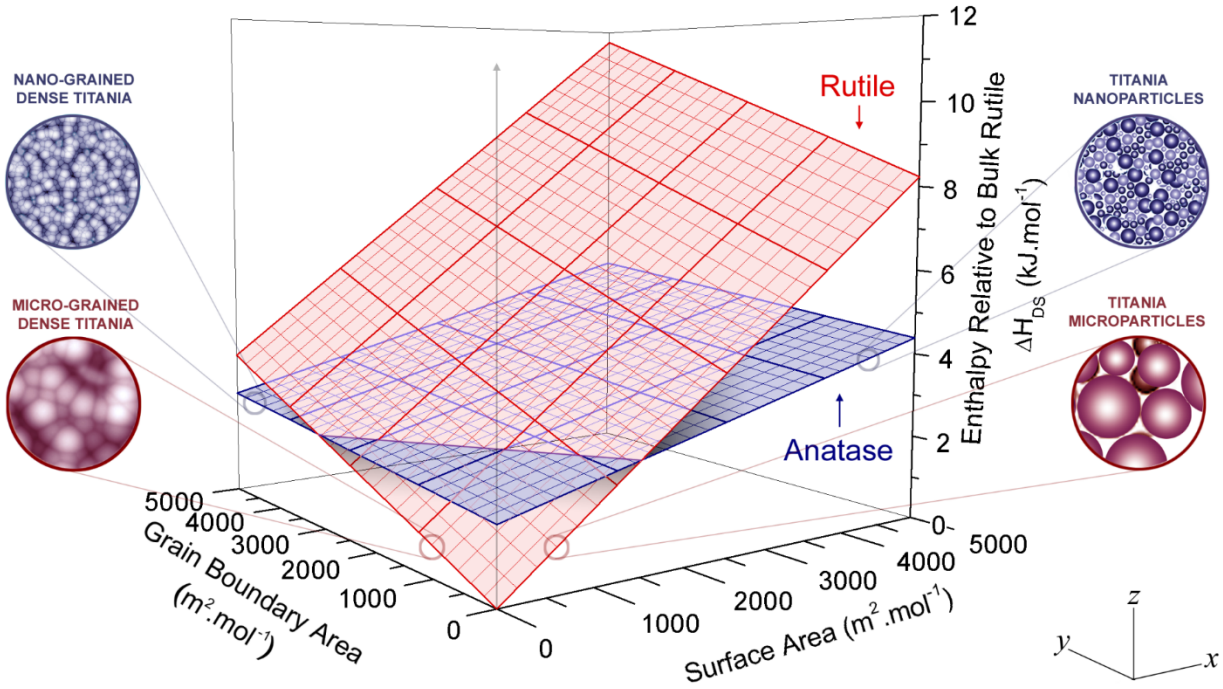

Figure 3. Stability diagram for nano-TiO_2 showing polymorphism dependent on both grain boundary and surface area due to the distinct specific energy of each. Darker plane represents anatase-phase enthalpy and lighter plane represents rutile-phase enthalpy. The crossover represents region of equal stability. Graph after Ref. 5.

That is, the surface term is only prevalent for nanoparticles which are fairly deagglomerated, without any solid-solid interfaces. However, it is not uncommon for particles to form necks and partially sinter during processing for most applications. This leads to the formation of grain boundaries with an excess energy that affects the overall free energy of the system and impacts polymorphism. Figure 3 shows the two extremes of fully deagglomerated particles and surface-free nanoceramics with only grain boundaries. Interestingly, the critical interfacial area indicating the cross-over of phase stability differs between the two extremes by about 1,500 m^2/mol. Under the assumption the specific interfacial energies are constant, the diagram predicts the relative stability of anatase to rutile at any surface to grain boundary area ratio, i.e. at different agglomeration states.

The knowledge of this dependence of phenomena such as phase transition (and coarsening) on the thermodynamics of interfaces is certainly not new. In the 1970's, Garvie et al. proposed the size dependent polymorphism of ZrO_2 to be a result of interfacial energetics; moreover, the complete theory of coarsening relies on the curvature driving force arising from excess interfacial energies [33, 34]. However, it was only in the past two decades that significant efforts were put into controlling the phenomena by targeting the modification of interfacial energies. It is not surprising from a physical-chemical perspective that interfacial energies are functions of composition. However, the intrinsic difficulties in separating kinetic and thermodynamic effects on microstructural evolutions raised questions about the impact of thermodynamics beyond being favorable or not. Because kinetics have exponential dependences, any energetic changes are usually assumed negligible in the big picture of processing. However, studies simulating mass transport during sintering of nanoparticles demonstrate the relevance of the thermodynamic extremal principle in connecting both kinetics and thermodynamics for the controlling (and understanding) of microstructural evolutions [35, 36]. The extremal principle states the energy of the system will evolve towards the pathway of fastest energy decay [37, 38]. In other words, during phenomena such as sintering, the combination of a specific diffusion coefficient and interfacial energy which delivers that fastest excess energy release rate will be responsible for governing the atomic movement. This simple statement constitutes the foundation of microstructure evolutions and shall serve as guideline for control.

2. Controlling interfacial energies

Fundamental descriptions of microstructural evolution in oxides state interfacial energies as constant driving forces [39]. However, Gibbs derived a thermodynamic relationship describing

the interdependence of the interface tension and solute excess (or adsorption per unit area). The relation can be written as $d\gamma = -\sum \Gamma \, d\mu_D$, where Γ is the number of moles of a component *D* which is adsorbed at the interface and $d\mu_D$ is the chemical potential difference caused by adsorption and is commonly referred to as 'adsorption isotherm'. Although this equation is typically applied in the context of surfactant ions or molecules being oriented and adsorbed on the interface of a liquid (such as sodium dodecyl sulfate in water), Gibbs derivation is not restricted to liquids, and several studies have further explored this relation in solids, particularly in metals [40]. This led to a modification of the equation which in the integral form takes the form of [41-43]:

$$\gamma = \gamma_0 - \Gamma[RTlnx - H_s] \quad (1)$$

This equation is derived for binary systems with solutes (dopants) prone to segregation, i.e. formation of interface excess. γ is the interfacial energy (either surface or grain boundary), γ_0 is the interfacial energy of the solid without the solute, the term $RTlnx$ accounts for the configurational entropy in an ideal dilute solution, and H_s is the enthalpy of segregation. A rigorous derivation of this equation has been provided by Weissmuller [44].

Equation 1 predicts a decrease in surface or grain boundary energy with segregation. This has been confirmed for a number of complex oxides by both atomistic simulations and experiments focusing to quantifying interface excess energies. **Figures 4 and 5** show a collections of experimental data on the effect of dopants on surface (Figure 4) and grain boundary (Figure 5) energies where interface excess is experimentally demonstrated (at least indirectly) [45-58]. The values are also listed in **Tables 1 and 2** for reference, as it may serve useful for the reader. Figures 4a and 5a show the absolute energy values attained from techniques ranging from water adsorption microcalorimetry to oxide melt drop solution calorimetry. The decrease in energy is a

function of dopant content and is apparently a general trend. A noteworthy data is provided for $MgAl_2O_4$ doped with 1mol% La which has several data points for the same concentration of dopant. The surface energies refer to several different grain sizes, ranging from 2.5nm (for the highest energy) up to 42nm (for the lowest energy) [46]. This is consistent with equation 1, and indicates Γ is affected both by the dopant content and by the interfacial area, i.e. the available space for segregation, which scales with the grain size.

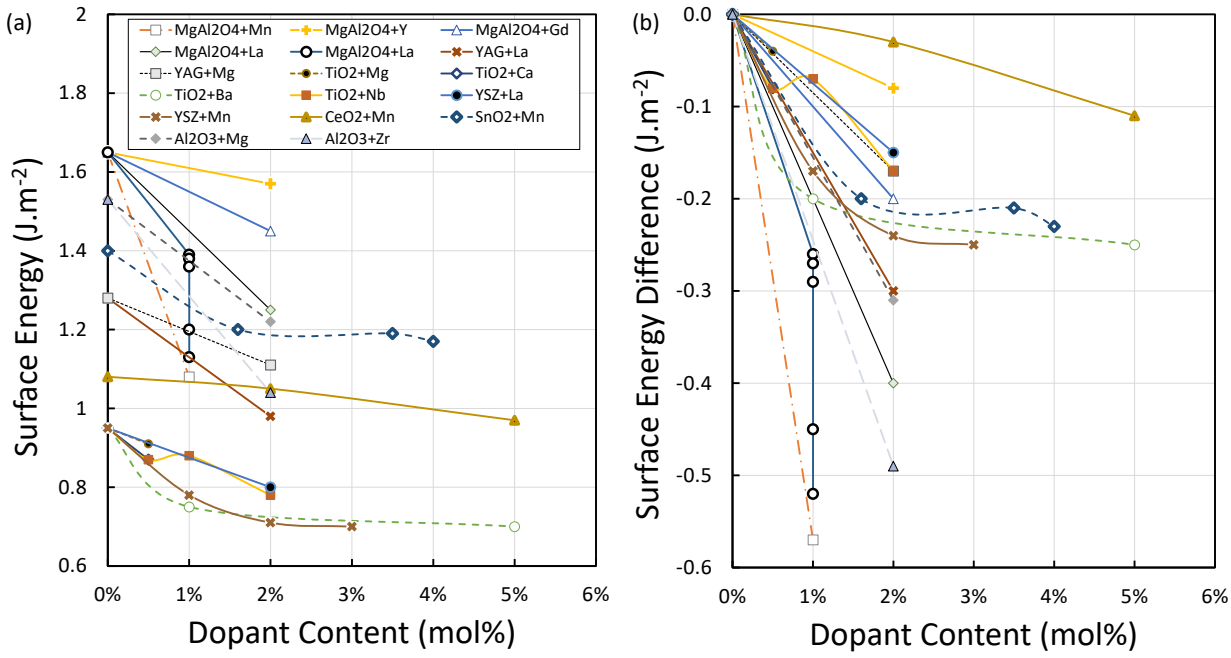

Figure 4. Surface energy as a function of dopant concentration for a variety of oxides as indicated in the legend. Data demonstrate a clear trend on the decrease of surface energy for absolute values in (a) and net difference in (b).

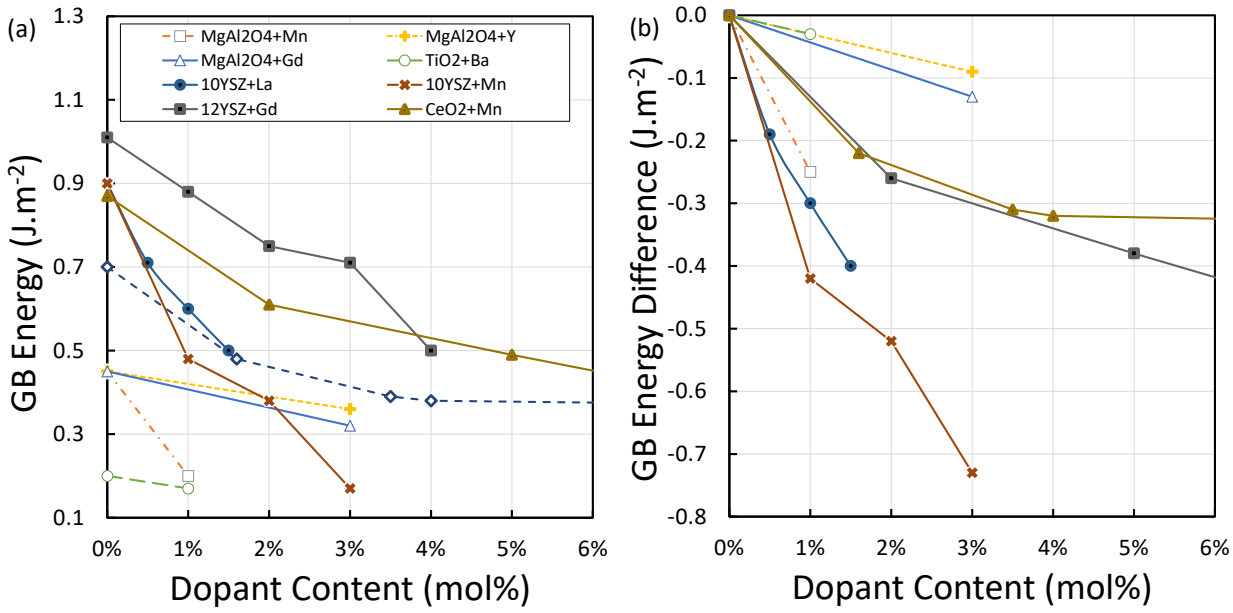

Figure 5. Grain boundary energy as a function of dopant concentration for a variety of oxides as indicated in the legend. Similar to surfaces, the data demonstrate a clear trend on the decrease of grain boundary energy for absolute values in (a) and net difference in (b).

Table 1. Surface energies from microcalorimetry for a series of oxides and dopants. Data is a collection from Refs. 45-58.

	Dopant	Conc. (mol%)	Surface Energies (J/m^2)	Size (nm)
$MgAl_2O_4$	-	-	1.65	
	La	1.0%	1.39	2.5
	La	1.0%	1.38	7.5
	La	1.0%	1.36	11
	La	1.0%	1.2	31
	La	1.0%	1.13	42
	Mn	1.0%	1.08	-
	Y	2.0%	1.57	-
	Gd	2.0%	1.45	-
	La	2.0%	1.25	-
YAG	-	-	1.28	-
	La	2.0%	0.98	-
	Mg	2.0%	1.11	-
a-TiO_2	-	-	0.95	-
	Mg	0.50%	0.91	-
	Ca	0.50%	0.87	-
	Ba	1.0%	0.75	-
	Ba	5.0%	0.7	-
	Ba	10.0%	0.73	-
	Nb	0.5%	0.87	-
	Nb	1.0%	0.88	-
	Nb	2.0%	0.78	-
YSZ	-	-	0.95	-
	La	2.0%	0.8	-
	Mn	1.0%	0.78	-
	Mn	2.0%	0.71	-
	Mn	3.0%	0.7	-
CeO_2	-	-	1.08	-
	Mn	2.0%	1.05	-
	Mn	5.0%	0.97	-
	Mn	10.0%	0.95	-
SnO_2	-	-	1.4	-
	Mn	1.6%	1.2	-
	Mn	3.5%	1.19	-
	Mn	4.0%	1.17	-
	Mn	8.5%	1.12	-
γ-Al_2O_3	-	-	1.53	-
	Mg	2.0%	1.22	-
	Zr	2.0%	1.04	-

Table 2. Grain boundary energies from microcalorimetry for a series of oxides and dopants. Data is a collection from Refs 45-58.

	Dopant	Conc. (mol%)	Grain Boundary Energies (J/m^2)
$MgAl_2O_4$	-	-	0.45
	Mn	1.0%	0.2
	Y	3.0%	0.36
	Gd	3.0%	0.32
a-TiO_2	-	-	0.2
	Ba	1.0%	0.17
10YSZ	-	-	0.9
	La	0.5%	0.71
	La	1.0%	0.6
	La	1.5%	0.5
10YSZ	-	-	0.9
	Mn	1.0%	0.48
	Mn	2.0%	0.38
	Mn	3.0%	0.17
12YSZ	-	-	1.01
	Gd	1.0%	0.88
	Gd	2.0%	0.75
	Gd	3.0%	0.71
	Gd	4.0%	0.5
CeO_2	-	-	0.87
	Mn	2.0%	0.61
	Mn	5.0%	0.49
	Mn	10.0%	0.3
SnO_2	-	-	0.7
	Mn	1.6%	0.48
	Mn	3.5%	0.39
	Mn	4.0%	0.38
	Mn	8.5%	0.37

The net energy differences for undoped versus doped compositions are highlighted in Figures 4b and 5b, evidencing the derivative and the total energy difference depends on both chemistries of the dopant and the host. For instance, while CeO_2 showed a mild decrease in the surface energy with Mn doping, $MgAl_2O_4$ showed a decrease of ~$0.59 J.m^{-2}$ for doping with 1mol% of the same

dopant [45, 59]. One can rationalize the discrepancy considering the dopant excess formation and the respective *energy of segregation*. From a physical chemistry perspective, segregation will be affected by ion-ion interactions, ionic size differences, as well as electrostatic interactions of the dopant ion with the host structure and space charge regions at both surface and grain boundaries [60]. Albeit focusing on aspects of grain boundary segregation, Wynblatt et al. [61] have provided a valuable description of possible parameters controlling the enthalpy of segregation (ΔH_s) valid for both surface and grain boundaries which can be written as:

$$\Delta H_s = \Delta H_\gamma + \Delta H_\omega + \Delta H_\varepsilon + \Delta H_\Phi \quad (2)$$

Here, ΔH_γ is the contribution to the enthalpy of segregation coming from the interfacial energies of the individual compounds (host and dopant), which is simply written as $[(\gamma_{host} - \gamma_{dopant}) \cdot A]$, with A being the area per mole of the solvent (host). ΔH_ω refers to the contribution due to solute-solvent interactions, and is given by:

$$\Delta H_\omega = \frac{\Delta H_{mix}}{Z^* X_h^b X_d^b} \quad (3)$$

This equation addresses the enthalpy of mixing (ΔH_{mix}), normalized for the coordination of ions at the interfaces (Z^*), and the molar fraction of the host and dopant in the bulk, X_h^b and X_d^b respectively. The term ΔH_ε relates to the elastic strain energy contribution, which takes into account mechanical properties of the components (K for bulk modulus and G for shear modulus) and their respective ionic radius ($r_h$or r_d), and is written approximately by:

$$\Delta H_\varepsilon = \frac{24\pi \mathrm{K G} r_h r_d (r_h r_d)^2}{4\mathrm{G} r_h + 3K r_d} \quad (4)$$

The last term ΔH_Φ is related to the electrostatic interactions between host and dopant, such that $\Delta H_\Phi = qe\Phi_\infty$, where q is the valence difference between ions, and Φ_∞ is the internal potential

away from the interface, which is simply the energy difference between the formation of a cation and an anion vacancy.

Although the equations 2-4 give a clearer picture of segregation dependences and should influence dopant selections in materials' design if one intends to control interfacial energies, an exact prediction of the dopant effect is still utopic. One complication is that the presented equations neglect possible interactions between terms. Moreover, in complex oxides it is known the vicinity of interfaces may incur significant reconstruction to accommodate excess energies, causing for instance the formation of vacancies and space charge layers, or affecting the degree of cationic site inversion, as recently described in $MgAl_2O_4$ [62-64]. Segregation of cations to the interface will disturb this local equilibrium which can hardly be described by the simplistic equations described above. In some cases, predicting segregation is difficult simply because of the dynamic nature of a system. For instance, Mn doping can be subjected to oxidation state changes during common processing conditions, affecting ionic radius and mechanical constants. This will affect its segregation enthalpy, which has been previously demonstrated to oscillate from favorable to unfavorable during programmed thermal annealing [65].

While the literature has some reports on enthalpy of segregation for complex oxides [66], equation 1 predicts a continuous decrease in interfacial energy with increasing dopant excess. The available data in Figures 4 and 5 show however that at relatively large concentrations, flattening of the curve is observed. This can be associated with the full occupation of the available interfacial sites by the segregated ions, creating a maximum value for Γ. Beyond such value, one may expect the formation of a precipitate of the dopant oxide, or a mixed oxide of host and dopant. In fact, the rules for the formation of a precipitate are not significantly different than the forces inducing segregation, and a competition between these too processes shall exist.

Consider an ion D as a dopant for a given host oxide. Each individual D ion has technically the possibility of being incorporated at an interface excess, or be part of a precipitate as a new phase, the chosen pathway being dictated by the energy decrease associated with each. If all atoms D are segregated to the interface forming excess Γ_D, the change in Gibbs free energy will be given by:

$$\Delta G_{D(s)} = a\Gamma_D \overline{\Delta G_{seg}} + a\gamma \quad (5)$$

Here, a is the area of the interface, which when multiplied by the excess gives the total number of atoms; and $\overline{\Delta G_{seg}}$ is the energy of segregation *per ion*. If the ions D precipitate instead, the change in energy will be given by:

$$\Delta G_{D(p)} = a\Gamma_D \overline{\Delta G_p} \quad (6)$$

Where $\overline{\Delta G_p}$ is the energy of precipitation per ion. This energy should include not only bulk enthalpies, but also the interfacial energies emerging from the nucleation of the new phase. In truth, this energy directly connects to the conventional theory of homogeneous nucleation, in which interfacial energies are a significant energy cost for precipitation, which will include metastable enrichments of dopants at the interface. Although difficult to provide accurate data to predict this 'saturation' state, experimental observations are common in the literature. For example, in the NiO-SnO_2 system, both SnO_2 and NiO rich sides showed segregation of the low concentration component to the surface (i.e. Sn segregates on NiO and Ni segregates on SnO_2), causing lowering of surface energy. The segregation is however limited by the formation of a second phase, as schematically represented in Figure 6 from Ref. [67]. On the SnO_2 rich side, the diagram shows surface segregation evidenced by the dark ring around the particles. As a saturation limit is achieved, and the nucleation of a second phase takes place, NiO nanoparticles themselves start to form. Interestingly, the experimental diagram was fairly symmetrical,

meaning the NiO rich side showed an equivalent behavior, although not at the same critical compositions. That is, NiO showed some level of SnO_2 segregation followed by SnO_2 precipitation after saturation. It is likely other systems shall have similar behavior, but the picture can easily get more complex as it would scale with, for instance, the number of potential phases and mixed oxides [67, 68].

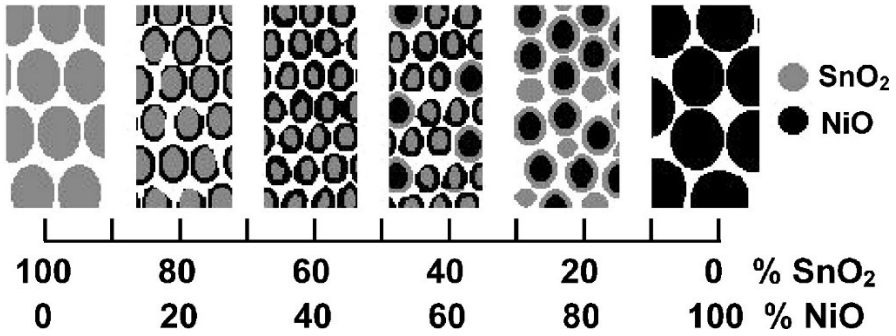

Figure 5. Schematic representation of the nanoparticles' morphology evolution with the composition of the NiO–SnO_2 system. On both SnO_2 and NiO rich sides, only one phase is present and the dopant (Ni or Sn, respectively), forms surface excess without precipitation. The precipitation occurs on both sides, but at different dopant contents. From Ref. 67.

3. Interfacial Energies in Oxide Phase Stability

The analysis of the whole composition spectrum in binary systems as shown in Figure 6 is very useful to understand how segregation fits in the context of phase stability at the nanoscale [69, 70]. Typical phase diagrams indicate equilibrium phases at given temperatures and compositions, assuming homogeneous solid solutions of the elements. Anything outside this is considered kinetically stabilized in a non-equilibrium state, which may be predicted by other tools such as experimental TTT diagrams. However, the extensive presence of interfaces in nanomaterials brings another possibility for ionic distribution which is not necessarily a simple kinetic trap.

Because the total energy of a system is a summation of bulk and interfacial energies, a simple oxide may find a low energy state at a given polymorph and grain size as a consequence of the surface energy of one of the polymorphs being lower, as discussed for alumina in Figure 1. In bi-cationic oxides (or in the case of a dopant), the energetic description is more complex, as the surface energies can be affected by the presence of a dopant, and so does the bulk. In bulk systems, the formation of a solid solution (i.e. a single phase) between two components is governed by the energy of mixing. For nanoscaled bi-cationic oxide systems with the general formula ABO, the surface energy contribution should be included in a modified enthalpy of mixing (ΔH_{mix}^{Nano}) described by:

$$\Delta H_{mix}^{Nano} = \Delta H_{mix} + \gamma_{ABO} \cdot SA_{ABO} - (\gamma_{AO} \cdot SA_{AO} + \gamma_{BO} \cdot SA_{BO}) \quad (7)$$

where γ_{ABO} is the surface energy of the 'solid solution', SA is the surface area of the nanocrystalline solid solution, and $\gamma_{AO},\ SA_{AO},\ \gamma_{BO},\ SA_{BO}$ the respective quantities for the oxides of cations A and B. In this context, the term 'solid solution' is used to describe a single phased material, even if surface excess exists. To simplify the problem description, this equation assumes the only possible phases to be formed are ABO, AO and BA, ignoring other phases with other AB stoichiometry. For the solid solution ABO to be stable, equation 7 needs to be exothermic, i.e. ≤ 0. In systems with *true* solid solution, and ions homogeneously distributed in the crystal volume, γ_{ABO} can be likely described by a rule of mixtures. However, if the lowest concentration cation is prone to segregation, γ_{BO} is governed by equation 1, meaning the surface energy will be lowered and will significantly increase the stability of the single phased region. This scenario fits well with the general story described in the diagram in Figure 6 for SnO_2-NiO, but the lack of proper thermodynamic data for most systems prevents the desirable quantifications and predictions.

Moreover, if one considers a more realistic description of nanoparticles, equation 7 needs additional terms describing the grain boundary contributions for all existing phases, as well as the hetero-interfaces naturally existing between each of the particles. Since equation 1 is applicable also for hetero-interfaces [71], the energy of segregation for each interface will be the competitive term defining the thermodynamic metastability of nanophases.

In other words, a key observation from equations 2-4 regarding the energy of segregation is that surfaces, grain boundaries and hetero-interfaces shall have distinct segregation driving forces for a given composition. Therefore, one may expect a dopant will distribute across all existing interfaces during synthesis and processing of nanoparticles in a way to minimize the total energy of the system. This doesn't mean the energy of segregation difference is the sole measure for this distribution pattern, but rather the combination of all interfacial areas and volumes instead. While phase stability is certainly affected by dopant segregation, even microstructures in single phased systems will be defined by how dopants distribute in "equilibrium".

For example, excluding the possibility of a second phase formation, the energy of a particulate system is the summation of all interfacial energies and bulk:

$$G = \gamma_S \cdot SA + \gamma_{gb} \cdot GBA + G_b \quad (8)$$

Here, γ is either surface or grain boundary energy as indicated in the subscript, and G_b is the energy of the bulk. SA and GBA are surface and grain boundary areas, respectively. In a doped system, this becomes:

$$G = \{\gamma_{s0} - \Gamma_s[RTlnx - H_s^s]\} \cdot SA + \{\gamma_{gb0} - \Gamma_{gb}\left[RTlnx - H_s^{gb}\right]\} \cdot GBA + G_{b(mix)} \quad (9)$$

Where we simply substituted equation 1 written for both surface and grain boundary (*s* or *gb* subscripts) into equation 8, and considered the effect of the dopant also on the bulk energy. H_s^s and H_s^{gb} refer to the enthalpy of segregation for the surface and grain boundary, respectively.

During processing, one may expect a dopant to distribute itself across the microstructure to minimize *G* in equation 9. This is not a trivial problem because not only the concentration of segregated dopants at SA and GBA can vary, but also SA and GBA themselves may change to accommodate more ions and potentially minimize the energy. Anyhow, equation 9 can be technically used to predict microstructures based on the energy dependences alone. That is, if all parameters and interdependences are known and if a 'solution' for this problem exists, it can predict interfacial areas and respective excesses in a minimal energy state. This would be a meta-equilibrium state, since the equilibrium condition still refers to the zero-interface solid, and its existence still depends on the overall diffusivity of the system. In truth, as discussed in the next sessions, kinetics will always play a key role in the microstructural stability and evolution regardless of the thermodynamic conditions.

3. Interfacial Energies in Coarsening Control

3.1. Effects on Grain Growth

Interfacial energies serve as the thermodynamic driving force for thermally activated coarsening phenomena. Although most coarsening control protocols found in the literature target kinetic parameters alone, such as reduction of mobility by introducing precipitates [72], it has been demonstrated that the control of interfacial energies can produce low energy metastable states which resist coarsening to a great extent during synthesis or processing at elevated temperatures [51, 52, 73, 74].

To understand the thermo-kinetic dependences, let's first address the problem of grain growth in the absence of surfaces. Grain growth is a thermally activated process driven by grain boundary energy. The local driving force is the grain boundary curvature which originates from the

equilibrium angles formed at the tripled joints and the geometrical constrains in the system [75]. The curvature creates a squared dependence of the grain size on the radius, with the conventional grain growth equation being written as:

$$d^2 - d_0^2 = k \cdot D_{gb}\gamma_{gb}t \quad (10)$$

Here, d is the grain size, d_0 its initial size, k a constant, D_{gb} and γ_{gb} are the diffusion and energy of the grain boundary, respectively. This equation has been the foundation for grain growth control for decades, and because of the exponential dependence behind D_{gb}, this is the most targeted control parameter, with mechanisms such as *solute-drag* neglecting the effect of segregated dopants on thermodynamics [76]. Contrasting this, Nafsin et al. attempted to demonstrate thermodynamics play a non-negligible role in grain growth by studying the consequences of the annihilation of the process' driving force. The work showed it is indeed possible to lower the grain boundary energy asymptotically to zero if a high concentration of dopant is segregated without the formation of a second phase [51]. By doping cubic zirconia (stabilized with 10 mol% Y, YSZ) with a fixed amount of Gd ions (4mol%), Nafsin et al. showed the γ_{gb} at grain sizes of 13nm is reduced from about 1J.m^{-2} for YSZ to about 0.5J.m^{-2}. Calorimetric data indicated γ_{gb} decreased with the increasing grain size, consistent with equation 1. That is, as the grain boundary area reduced due to grain growth, the net concentration of Gd at the grain boundaries increases as schematically represented in **Figure 7a**. This leads to a reduction of grain boundary energy because of the excess term (Γ) increase (refer to equation 1). The data showed the grain boundary energy decreased asymptotically to ~0.05 J.m^{-2}, as shown in **Figure 7b**, and this value is achieved approximately at the grain sizes around 55nm. Putting this in the perspective of equation 8, one may suggest ~0.05J.m^{-2} constitutes a negligible driving force for grain growth, and though atomic mobility may exist, there would be no net movement

of the boundary itself. As the doped system was subjected to annealing at 1100 °C for different times, the grains grew up to 54 nm but leveled at this size range after 16h of annealing. **Figure 7c** shows the grain sizes as a function of annealing time for both YSZ and Gd-doped YSZ evidencing the difference in growth and the plateau caused by Gd doping. The coincidence between the “zero grain boundary energy” grain size and this growth behavior is intriguing.

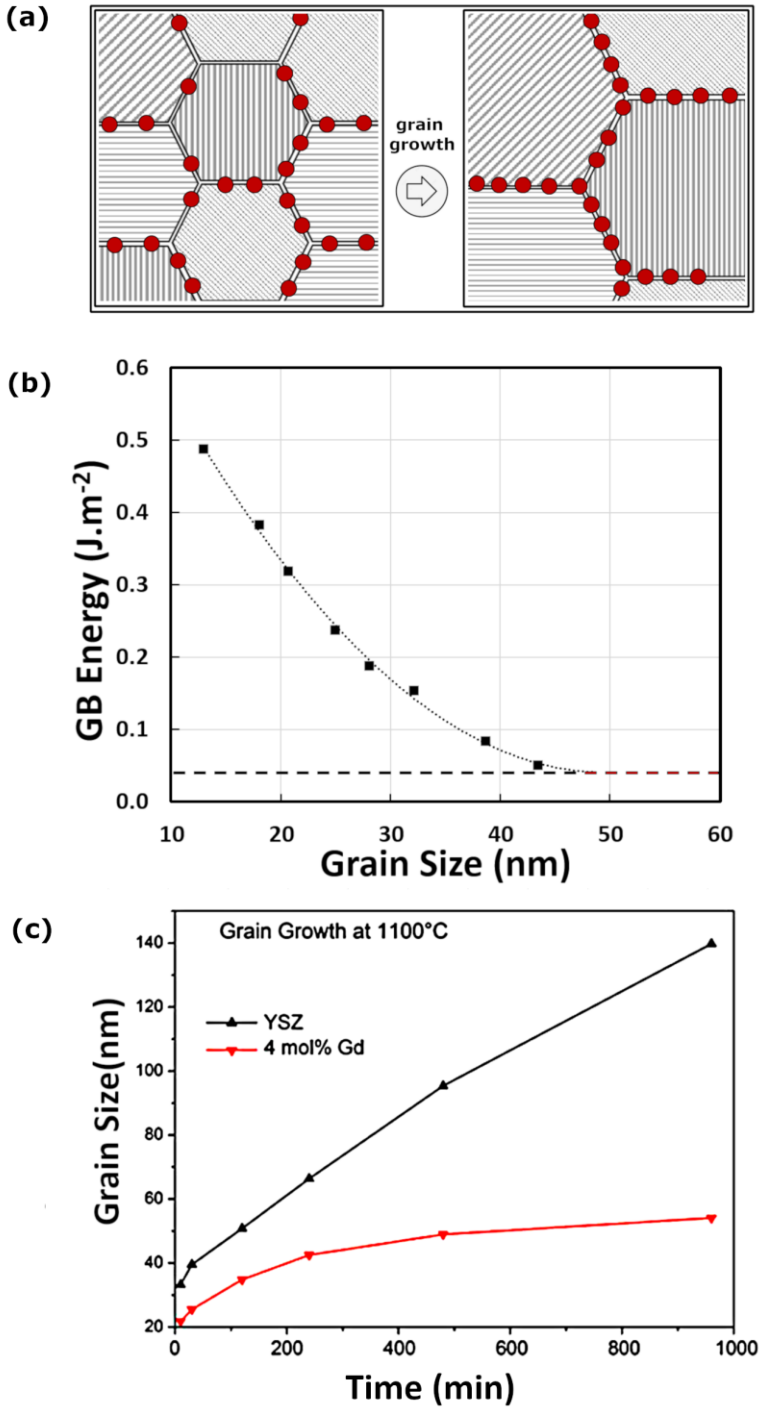

Figure 7. (a) Schematic representation of the effect of grain size on the excess term. Red circles represent segregated Gd ions. Because the number of segregated Gb ions do not change, a reduction in grain boundary area causes increase in Γ. (b) Grain boundary energy as a function of grain size showing an asymptotic decrease down to

0.05J/m^{-2}. Replotted from Ref. 51 (c) Grain growth behavior of YSZ and 4 mol% Gd doped YSZ at 1100 °C adapted from Ref. 51. Plateau is observed as the grain boundary energy is reduced to practically zero.

Furthermore, a parallel work demonstrated the mobility of the grain boundary at 1100 °C is absolutely not negligible for this system, and Gd addition to YSZ has actually minimal influence in the activation energy of grain growth (<0.09eV) [52], this proves a non-negligible role of thermodynamics in grain growth control of oxides as theoretically described in details elsewhere [77]. To be fair, this does not mean all systems shall behave similarly to Gd-doped YSZ, particularly because achieving high concentrations of segregates to interfaces is limited by the potential to form a second phase, as described in equations 5 and 6, but the example points out a thermo-kinetic approach provides the only appropriate strategy for a comprehensive grain growth analysis.

3.2. Effects on Coalescence and Sintering

The effect of interfacial energies has also been explored in the context of sintering and coalescence of oxides. Coarsening of nanoparticles is a critical aspect for their application in moderate temperatures, and it is not uncommon to observe particle enlargement during utilization of nanoparticles in fuel cells [78] or even in battery materials [79]. Coalescence by Ostwald ripening has as the main driving force the elimination of the surface to reduce excess energy, following an equation similar to equation 10 but with a cubic dependence on time instead, being typically written as [80]:

$d^3 - d_0^3 = k \cdot t$, where $k = \frac{3Dc_o\gamma M}{4\rho RT}$ (11)

where c_o is the equilibrium solubility, d is the particle radius, D is the diffusion coefficient of the active mechanism (e.g. surface diffusion), γ is the surface energy and ρ the material density. R and T have usual meaning. In this framework, the variables that may be modified by a dopant are the diffusion coefficient and the surface energy. If an additive increases diffusion, particle growth would be favorable, and vice-versa. On the other hand, the surface energy could also be controlled and, if the surface energy decreased while the bulk energy is constant, the particle size would decrease in order to raise the ratio between surface energy and bulk volume energy. Hasan et al. demonstrated such coarsening control by targeting lowering of the surface energy of $MgAl_2O_4$ using rare earths as dopants [55]. **Figure 8** shows the effect of Y, Gd or La ions used at 2 mol%. A remarkable reduction of the surface energy is observed, going from 1.65 $J.m^{-2}$ for undoped $MgAl_2O_4$ nanoparticles down to 1.27 $J.m^{-2}$ for La-doped $MgAl_2O_4$. There is a clear dependence of the energy reduction on the ionic radius, which was also confirmed by atomistic simulations in terms of enthalpy of segregation. This is aligned with stated dependences of the enthalpy of segregation as highlighted in equation 2. Noteworthy, the reduced surface energy indeed allowed for a 1.5 X increase in surface area for $MgAl_2O_4$ at a given temperature, persisting at ~180 $m^2.g^{-1}$ at 800°C for several hours, while the undoped composition showed reduction to ~120 $m^2.g^{-1}$ under similar conditions. This apparent success of thermodynamic inhibition of coalescence is however still limited by temperature. As temperatures rise, the stabilization of the surface energy is not sufficient to avoid coarsening because the system still possesses a positive excess energy. That is, the stabilization constitutes a meta-equilibrium state, and when diffusion paths are activated, the system is allowed to coarsens to its bulk counterpart. However, this high temperature step would now be intimately related to the process of sintering instead.

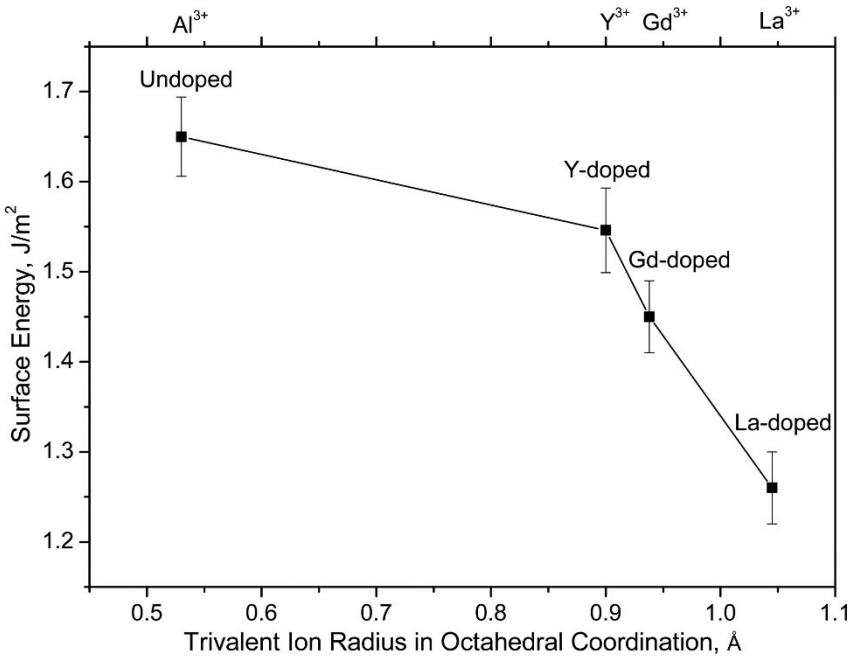

Figure 8. Surface energy measured by water adsorption microcalorimetry of undoped $MgAl_2O_4$ and Y-, Gd-, and La-doped $MgAl_2O_4$ as a function of trivalent ion radius from Ref. 51.

Differently than coalescence, sintering involves the concomitant evolution of both grain boundary and surfaces, which requires the analysis of the effect of dopants at both interfaces. Sintering is a process of surface elimination accompanied by the formation (and subsequent elimination) of grain boundaries, so the energy evolution during the process can be described as:

$$\Delta G = \Delta(\gamma_s dA_s) + \Delta(\gamma_{gb} dA_{gb}) \quad (12)$$

Here, the surface area evolution dA_s is generally negative, but the grain boundary area change dA_{gb} can be positive at the beginning of sintering and later become negative when grain growth takes place. Li et al. studied the effect of La as a dopant in YSZ, focusing on how the thermodynamic changes affects the sintering behavior [81]. 2 mol% La was sufficient to decrease the surface energy of YSZ from 0.95 to 0.7 $J.m^{-2}$, with a reduction of the grain boundary energy from 0.8 to 0.4 $J.m^{-2}$. While a decrease in coalescence is expected due to the

surface energy reduction, because the dihedral angle (or equilibrium angle,φ_e) is related to the interfacial energies by the Young's equation, $\gamma_{gb} = 2\gamma_s cos(\varphi_e/2)$, [82] one may calculate a change in dihedral angle from 137 to 150°, meaning a great increase in sintering stress [83, 84]. Sintering "stress" technically defines a particulate system's potential for sintering, and includes the curvature potential and the difference between the system's energy when particles are at a given contact angle and its energy when the angle reaches the dihedral angle. As a rule, the larger the dihedral angle is, the greater the sintering stress as it translates into more energy reduction during the process. However, Li et al. further reported densification was not improved in La-doped YSZ despite the more favorable driving force. This implies that in sintering, a favorable thermodynamics is a necessary but not sufficient condition for densification enhancement, as was later discussed in the context of the extremal principal [85]. This disconnect between sintering stress and actual densification is reasoned by the effective diffusivity. Although increased sintering stress can lead to more densification at the first stages of sintering, when mechanisms such as surface diffusion are active, the system will eventually be trapped at a metastable condition as a consequence of the limited mobility at the grain boundaries. Late stages of sintering are characterized by densification accompanied by grain growth, one being fundamentally connected to the other [83]. If the latter is stopped, the sintering may enter another meta-equilibrium state. Similarly to Gd doped YSZ (Figure 7b), La also reduces the grain boundary energy of YSZ, causing the grain boundaries to virtually stop and retard densification. This thermo-kinetic connection can be easily visualized by contrasting with another dopant. Mn doped YSZ showed a similar increase in dihedral angle, but an enhanced diffusivity caused by grain boundary defects induced by Mn oxidation state change during sintering [86]. This led to enhanced densification, also followed by significant grain growth. A

similar effect was observed in Mn doped $MgAl_2O_4$ [45], which shows reduced densification temperature in contrast to the undoped phase. **Figure 9** shows a very simplified diagram of possible microstructural evolutions considering both sintering stress and mobility dependences. Despite simplicity, this diagram helps understanding the microstructural dependences during sintering. It is tempting to connect this diagram to the more usual "mass transport mechanisms' theory of sintering, but unfortunately, quantitative prediction of diffusion enhancements caused by dopant is also not trivial, and process optimization still rely on extensive literature data, or perhaps should rely on machine learning in the near future.

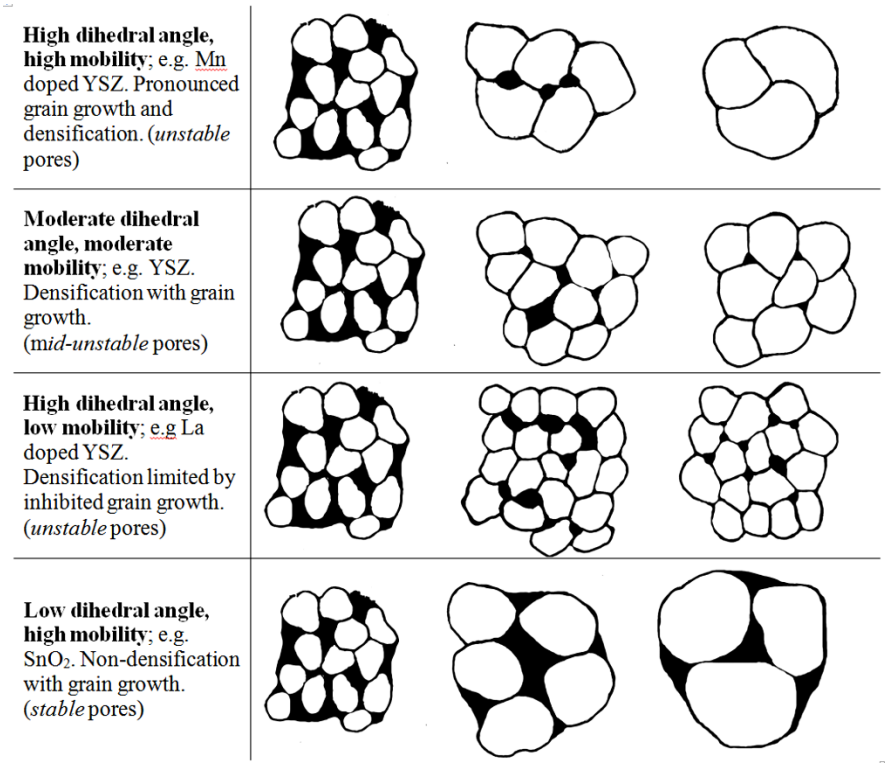

Figure 9. Schematic representation of microstructural evolutions (pore/grain size) at different stages of sintering as a function of thermodynamic and kinetic conditions. Black regions identify porosity. From Ref. 82.

Summary

This work summarizes some aspects of interfacial energy effects on the microstructural evolution of nanocrystalline complex oxides. Because interfaces account for a large fraction of the atomic volume at the nanoscale, a comprehensive thermodynamic description must include terms related to surfaces and grain boundaries. Unfortunately, there is only limited data on experimental interfacial energies, but recent advances in experimental thermodynamics combined with atomistic simulations have suggested new routes to design and control nanocrystalline oxides fundamentally targeting interfacial energies.

Although we focused on average interfacial energies in contrast to energies specific for individual planes or orientations, the meaningful collection of data suggest this simplified perception is still valid and useful in microstructure control. Experimental data for individual surface planes would be certainly desirable for a true comprehensive description, but it constitutes a great challenge from the experimental perspective.

For relatively low temperature processes, there is evidence the energetics of interfaces are dominant factors in controlling phenomena such as coarsening (nanostability) and polymorphic stability at the nanoscale. In Ostwald ripening, although the surface energy has been present in the originally proposed analytical models, we have described it as a tunable parameter through the usage of dopants prone to surface segregation. A model for dopant selection based on enthalpy of segregation does exist, but it is still far from flawless. Similarly, phase diagrams for the nanoscale include interfacial energies and their variations with composition and segregation. Unfortunately, there is only available data to build a handful of these predictive diagrams, but those already suggest the power of thermodynamic knowledge in designing refined stable nanostructured oxides.

For relatively high temperature processes, such as sintering and grain growth, thermodynamics also plays a key role, but this is intrinsically connected to the more present diffusion mechanisms in the context of the thermodynamic extremal principle. As atomic movement happens towards the pathway of maximum energy reduction rate, the combination of interfacial energies and diffusion coefficients will define mechanisms of densification (or non-densification) during sintering. In grain growth, it has been demonstrated it is possible to practically eliminate growth driving force by targeting the reduction of grain boundary energies through dopant segregation. This represents a paradigm shift in traditional kinetic-only description of this process, but ignoring the role of dopants also in the defect chemistry and consequences in diffusion would be an equal mistake.

Acknowledgements

NSF DMR Ceramics 2015650.

References

[1] C. Jiang, E. Hosono, H. Zhou, Nanomaterials for lithium ion batteries, Nano today 1(4) (2006) 28-33.
[2] M. Hasan, J. Drazin, S. Dey, R.H.R. Castro, Synthesis of stoichiometric nickel aluminate spinel nanoparticles, American Mineralogist 100(2-3) (2015) 652-657.
[3] P. Kalita, S. Ghosh, G. Gutierrez, P. Rajput, V. Grover, G. Sattonnay, D.K. Avasthi, Radiation tolerance: Nano triumphs bulk, arXiv preprint arXiv:1912.11359 (2019).
[4] A. Navrotsky, Thermochemistry of nanomaterials, in: J.F. Banfield, A. Navrotsky (Eds.), Reviews in Mineralogy and Geochemistry: Nanoparticles and the Environment, Mineralogical Society of America and the Geochemical Society, Washington, 2001, pp. 73-103.
[5] R.H.R. Castro, B.B. Wang, The Hidden Effect of Interface Energies in the Polymorphic Stability of Nanocrystalline Titanium Dioxide, Journal of the American Ceramic Society 94(3) (2011) 918-924.
[6] R. Schlögl, S.B. Abd Hamid, Nanocatalysis: mature science revisited or something really new?, Angewandte Chemie International Edition 43(13) (2004) 1628-1637.
[7] K.C. Bedin, A.L.M. Freitas, A. Tofanello, I. Rodríguez-Gutiérrez, F.L. Souza, Revealing the synergy of Sn insertion in hematite for next-generation solar water splitting nanoceramics, International Journal of Ceramic Engineering & Science 2(5) (2020) 204-227.
[8] D.N. Muche, J.W. Drazin, J. Mardinly, S. Dey, R.H. Castro, Colossal grain boundary strengthening in ultrafine nanocrystalline oxides, Materials Letters 186 (2017) 298-300.

[9] A. Bokov, S.L. Zhang, L. Feng, S.J. Dillon, R. Faller, R.H.R. Castro, Energetic design of grain boundary networks for toughening of nanocrystalline oxides, J. Eur. Ceram. Soc. 38(12) (2018) 4260-4267.
[10] A. Bokov, J.A. Aguiar, M.L. Gong, A. Nikonov, R.H.R. Castro, A Strategy to Mitigate Grain Boundary Blocking in Nanocrystalline Zirconia, J. Phys. Chem. C 122(46) (2018) 26344-26352.
[11] N.A. Gaida, N. Nishiyama, O. Beermann, U. Schürmann, A. Masuno, C. Giehl, K. Niwa, M. Hasegawa, S. Bhat, R. Farla, L. Kienle, Microstructural effects on hardness and optical transparency of birefringent aluminosilicate nanoceramics, International Journal of Ceramic Engineering & Science 2(2) (2020) 76-82.
[12] H. Gleiter, Nanostructured materials: basic concepts and microstructure, Acta materialia 48(1) (2000) 1-29.
[13] A. Navrotsky, C. Ma, K. Lilova, N. Birkner, Nanophase transition metal oxides show large thermodynamically driven shifts in oxidation-reduction equilibria, Science 330(6001) (2010) 199-201.
[14] S.V. Ushakov, A. Navrotsky, Direct measurements of water adsorption enthalpy on hafnia and zirconia surfaces using novel design for gas adsorption microcalorimetry, Applied Physics Letters 87(16) (2005) Art. No. 164103.
[15] J.M. McHale, A. Auroux, A.J. Perrotta, A. Navrotsky, Surface energies and thermodynamic phase stability in nanocrystalline aluminas, Science 277(5327) (1997) 788-791.
[16] R.H.R. Castro, On the thermodynamic stability of nanocrystalline ceramics, Materials Letters 96 (2013) 45-56.
[17] K. Kendall, N.M. Alford, J. Birchall, A new method for measuring the surface energy of solids, Nature 325(6107) (1987) 794.
[18] M.M. Hasan, P.P. Dholabhai, R.H.R. Castro, B.P. Uberuaga, Stabilization of MgAl2O4 spinel surfaces via doping, Surf. Sci. 649 (2016) 138-145.
[19] N.H. de Leeuw, F.M. Higgins, S.C. Parker, Modeling the surface structure and stability of alpha-quartz, Journal of Physical Chemistry B 103(8) (1999) 1270-1277.
[20] G.W. Watson, E.T. Kelsey, N.H. deLeeuw, D.J. Harris, S.C. Parker, Atomistic simulation of dislocations, surfaces and interfaces in MgO, Journal of the Chemical Society-Faraday Transactions 92(3) (1996) 433-438.
[21] P.M. Oliver, G.W. Watson, S.C. Parker, Molecular-dynamics simulations of nickel oxide surfaces, Physical Review B 52(7) (1995) 5323-5329.
[22] S. Blonski, S.H. Garofalini, MOLECULAR-DYNAMICS SIMULATIONS OF ALPHA-ALUMINA AND GAMMA-ALUMINA SURFACES, Surf. Sci. 295(1-2) (1993) 263-274.
[23] M. Baudin, M. Wojcik, K. Hermansson, Dynamics, structure and energetics of the (111), (011) and (001) surfaces of ceria, Surf. Sci. 468(1-3) (2000) 51-61.
[24] N.H. de Leeuw, J.A. Purton, S.C. Parker, G.W. Watson, G. Kresse, Density functional theory calculations of adsorption of water at calcium oxide and calcium fluoride surfaces, Surf. Sci. 452(1-3) (2000) 9-19.
[25] A. Navrotsky, Progress and new directions in calorimetry: A 2014 perspective, Journal of the American Ceramic Society 97(11) (2014) 3349-3359.
[26] J.W. Drazin, R.H.R. Castro, Water Adsorption Microcalorimetry Model: Deciphering Surface Energies and Water Chemical Potentials of Nanocrystalline Oxides, J. Phys. Chem. C 118(19) (2014) 10131-10142.
[27] D.V. Quach, A.R. Bonifacio, R.H.R. Castro, Water adsorption and interface energetics of zinc aluminate spinel nanoparticles: Insights on humidity effects on nanopowder processing and catalysis, J. Mater. Res. 28(15) (2013) 2004-2011.
[28] A.A. Levchenko, G. Li, J. Boerio-Goates, B.F. Woodfield, A. Navrotsky, TiO2 stability landscape: Polymorphism, surface energy, and bound water energetics, Chemistry of Materials 18(26) (2006) 6324-6332.
[29] G. Sharma, S.V. Ushakov, A. Navrotsky, Size driven thermodynamic crossovers in phase stability in zirconia and hafnia, Journal of the American Ceramic Society 101(1) (2018) 31-35.

[30] J.W. Drazin, R.H.R. Castro, Phase Stability in Nanocrystals: A Predictive Diagram for Yttria-Zirconia, Journal of the American Ceramic Society 98(4) (2015) 1377-1384.
[31] J.W. Drazin, R.H.R. Castro, Phase Stability in Calcia-Doped Zirconia Nanocrystals, Journal of the American Ceramic Society 99(5) (2016) 1778-1785.
[32] R.L. Grosso, E.N.S. Muccillo, R.H.R. Castro, Phase stability in scandia-zirconia nanocrystals, Journal of the American Ceramic Society 100(5) (2017) 2199-2208.
[33] R.C. Garvie, M.V. Swain, Thermodynamics of the tetragonal to monoclinic phase transformation in constrained zirconia microcrystals, Journal of materials science 20(4) (1985) 1193-1200.
[34] R. Garvie, Stabilization of the tetragonal structure in zirconia microcrystals, The Journal of Physical Chemistry 82(2) (1978) 218-224.
[35] F. Abdeljawad, D.S. Bolintineanu, A. Cook, H. Brown-Shaklee, C. DiAntonio, D. Kammler, A. Roach, Sintering processes in direct ink write additive manufacturing: A mesoscopic modeling approach, Acta Materialia 169 (2019) 60-75.
[36] J.M. Sestito, F. Abdeljawad, T.A. Harris, Y. Wang, A. Roach, An atomistic simulation study of nanoscale sintering: The role of grain boundary misorientation, Computational Materials Science 165 (2019) 180-189.
[37] M.M. Gong, R.H.R. Castro, F. Liu, Modeling grain growth kinetics of binary substitutional alloys by the thermodynamic extremal principle, Journal of Materials Science 50(13) (2015) 4610-4621.
[38] F. Fischer, J. Svoboda, H. Petryk, Thermodynamic extremal principles for irreversible processes in materials science, Acta Materialia 67 (2014) 1-20.
[39] S.-J.L. Kang, Sintering: densification, grain growth & microstructure, Elsevier, New York, 2005.
[40] T. Chookajorn, H.A. Murdoch, C.A. Schuh, Design of Stable Nanocrystalline Alloys, Science 337(6097) (2012) 951-954.
[41] R. Kirchheim, Reducing grain boundary, dislocation line and vacancy formation energies by solute segregation. I. Theoretical background, Acta Materialia 55(15) (2007) 5129-5138.
[42] F. Liu, R. Kirchheim, Nano-scale grain growth inhibited by reducing grain boundary energy through solute segregation, Journal of crystal growth 264(1-3) (2004) 385-391.
[43] R. Kirchheim, Grain coarsening inhibited by solute segregation, Acta Materialia 50(2) (2002) 413-419.
[44] J. Weissmuller, Alloy effects in nanostructures, Nanostructured Materials 3(1-6) (1993) 261-272.
[45] K. Nakajima, H. Li, N. Shlesinger, J.B.R. Neto, R.H.R. Castro, Low-temperature sintering of magnesium aluminate spinel doped with manganese: Thermodynamic and kinetic aspects, Journal of the American Ceramic Society 103(8) (2020) 4167-4177.
[46] D.N.F. Muche, A.L. da Silva, K. Nakajima, D. Gouvea, R.H.R. Castro, Simultaneous segregation of lanthanum to surfaces and grain boundaries in MgAl2O4 nanocrystals, Applied Surface Science 529 (2020).
[47] G. Sharma, K. Nakajima, D.N.F. Muche, R.H.R. Castro, The influence of dopants on the surface enthalpy of Yttrium aluminum garnet (YAG), Thermochimica Acta 683 (2020).
[48] A.L. da Silva, D.N.F. Muche, L.B. Caliman, J. Bettini, R.H.R. Castro, A. Navrotsky, D. Gouvea, TiO2 Surface Engineering to Improve Nanostability: The Role of Interface Segregation, J. Phys. Chem. C 123(8) (2019) 4949-4960.
[49] M.M. Hasan, P.P. Dholabhai, S. Dey, B.P. Uberuaga, R.H.R. Castro, Reduced grain boundary energies in rare-earth doped MgAl2O4 spinel and consequent grain growth inhibition, J. Eur. Ceram. Soc. 37(13) (2017) 4043-4050.
[50] L.J. Wu, P.P. Dholabhai, B.P. Uberuaga, R.H.R. Castro, Temperature Dependence Discontinuity in the Stability of Manganese-Doped Ceria Nanocrystals, Cryst. Growth Des. 17(2) (2017) 446-453.
[51] N. Nafsin, R.H.R. Castro, Direct measurements of quasi-zero grain boundary energies in ceramics, J. Mater. Res. 32(1) (2017) 166-173.

[52] N. Nafsin, J.A. Aguiar, T. Aoki, A.M. Thron, K. van Benthem, R.H.R. Castro, Thermodynamics versus kinetics of grain growth control in nanocrystalline zirconia, Acta Materialia 136 (2017) 224-234.
[53] A.L. da Silva, D. Hotza, R.H.R. Castro, Surface energy effects on the stability of anatase and rutile nanocrystals: A predictive diagram for Nb2O5-doped-TiO2, Applied Surface Science 393 (2017) 103-109.
[54] M.M. Hasan, P.P. Dholabhai, R.H. Castro, B.P. Uberuaga, Stabilization of MgAl2O4 spinel surfaces via doping, Surf. Sci. 649 (2016) 138-145.
[55] M.M. Hasan, S. Dey, N. Nafsin, J. Mardinly, P.P. Dholabhai, B.P. Uberuaga, R.H.R. Castro, Improving the Thermodynamic Stability of Aluminate Spinel Nanoparticles with Rare Earths, Chemistry of Materials 28(14) (2016) 5163-5171.
[56] R.H.R. Castro, D. Gouvea, Sintering and Nanostability: The Thermodynamic Perspective, Journal of the American Ceramic Society 99(4) (2016) 1105-1121.
[57] C.H. Chang, S. Dey, R.H.R. Castro, Energetics of Oriented Attachment of Mn-Doped SnO2 Nanoparticles, J. Phys. Chem. C 119(35) (2015) 20662-20672.
[58] L.J. Wu, S. Dey, M.M. Gong, F. Liu, R.H.R. Castro, Surface Segregation on Manganese Doped Ceria Nanoparticles and Relationship with Nanostability, Journal of Physical Chemistry C 118(51) (2014) 30187-30196.
[59] L.J. Wu, J.A. Aguiar, P.P. Dholabhai, T. Holesinger, T. Aoki, B.P. Uberuaga, R.H.R. Castro, Interface Energies of Nanocrystalline Doped Ceria: Effects of Manganese Segregation, J. Phys. Chem. C 119(49) (2015) 27855-27864.
[60] W.C. Mackrodt, P.W. Tasker, Segregation Isotherms at the Surfaces of Oxides, Journal of the American Ceramic Society 72(9) (1989) 1576-1583.
[61] P. Wynblatt, G.S. Rohrer, F. Papillon, Grain boundary segregation in oxide ceramics, J. Eur. Ceram. Soc. 23(15) (2003) 2841-2848.
[62] B.P. Uberuaga, R. Perriot, Spatially-varying inversion near grain boundaries in MgAl 2 O 4 spinel, RSC Advances 10(20) (2020) 11737-11742.
[63] D.N.F. Muche, M.A.T. Marple, I. Hung, Z.H. Gan, R.H.R. Castro, S. Sen, Size-Induced Structural Disorder Enables Ultrahard Oxides, J. Phys. Chem. C 121(25) (2017) 13898-13905.
[64] D.N.F. Muche, M.A.T. Marple, S. Sen, R.H.R. Castro, Grain boundary energy, disordering energy and grain growth kinetics in nanocrystalline MgAl2O4 spinel, Acta Materialia 149 (2018) 302-311.
[65] C.-H. Chang, J.F. Rufner, K. van Benthem, R.H.R. Castro, Design of Desintering in Tin Dioxide Nanoparticles, Chemistry of Materials 25(21) (2013) 4262-4268.
[66] P. Lejček, M. Všianská, M. Šob, Recent trends and open questions in grain boundary segregation, J. Mater. Res. 33(18) (2018) 2647-2660.
[67] R.H.R. Castro, P. Hidalgo, R. Muccillo, D. Gouvea, Microstructure and structure of NiO-SnO2 and Fe2O3-SnO2 systems, Applied Surface Science 214(1-4) (2003) 172-177.
[68] W.M. Carvalho, L. Mendonca-Ferreira, F.N. Costa, F.F. Ferreira, D.N.F. Muche, R.A. Tofanello, R.H.R. Castro, F.L. Souza, Annealing control of hydrothermally grown hematite nanorods: Implication of structural changes and Cl concentration on weak ferromagnetism, Journal of Alloys and Compounds 799 (2019) 83-88.
[69] J. Miagava, A. Rubbens, P. Roussel, A. Navrotsky, R.H.R. Castro, D. Gouvêa, The Nanocrystalline SnO2–TiO2 System—Part I: Structural Features, Journal of the American Ceramic Society (2015) n/a-n/a.
[70] J. Miagava, A.L. da Silva, A. Navrotsky, R.H.R. Castro, D. Gouvêa, The Nanocrystalline SnO2–TiO2 System–Part II: Surface Energies and Thermodynamic Stability, Journal of the American Ceramic Society (2015) n/a-n/a.
[71] L.J. Wu, S. Dey, J. Mardinly, M. Hasan, R.H.R. Castro, Thermodynamic Strengthening of Heterointerfaces in Nanoceramics, Chemistry of Materials 28(9) (2016) 2897-2901.
[72] S.A. Humphry-Baker, C.A. Schuh, Suppression of grain growth in nanocrystalline Bi2Te3 through oxide particle dispersions, Journal of Applied Physics 116(17) (2014) 173505.

[73] G. Oskam, Z. Hu, R.L. Penn, N. Pesika, P.C. Searson, Coarsening of metal oxide nanoparticles, Physical Review E 66(1) (2002) 011403.
[74] Z. Hu, G. Oskam, R.L. Penn, N. Pesika, P.C. Searson, The influence of anion on the coarsening kinetics of ZnO nanoparticles, The Journal of Physical Chemistry B 107(14) (2003) 3124-3130.
[75] S.-J.L. Kang, Sintering: densification, grain growth and microstructure, Elsevier2004.
[76] I.W. Chen, Mobility Control of Ceramic Grain-Boundary and Interfaces, Mater. Sci. Eng. A-Struct. Mater. Prop. Microstruct. Process. 166(1-2) (1993) 51-58.
[77] H. Peng, Z. Jian, F. Liu, Review of thermo-kinetic correlation during grain growth in nanocrystalline materials, International Journal of Ceramic Engineering & Science 2(2) (2020) 49-65.
[78] A. Kregar, A. Kravos, T. Katrašnik, Methodology for Evaluation of Contributions of Ostwald Ripening and Particle Agglomeration to Growth of Catalyst Particles in PEM Fuel Cells, Fuel Cells 20(4) (2020) 487-498.
[79] J.P. Pender, G. Jha, D.H. Youn, J.M. Ziegler, I. Andoni, E.J. Choi, A. Heller, B.S. Dunn, P.S. Weiss, R.M. Penner, Electrode degradation in lithium-ion batteries, ACS nano 14(2) (2020) 1243-1295.
[80] G.J. Pereira, R.H.R. Castro, P. Hidalgo, D. Gouvea, Surface segregation of additives on SnO2 based powders and their relationship with macroscopic properties, Applied Surface Science 195(1-4) (2002) 277-283.
[81] H. Li, S. Dey, R.H.R. Castro, Kinetics and thermodynamics of densification and grain growth: Insights from lanthanum doped zirconia, Acta Materialia 150 (2018) 394-402.
[82] B.J. Kellett, F.F. Lange, Thermodynamics of densification .1. Sintering of simple particle arrays, equilibrium-configurations, pore stability, and shrinkage, Journal of the American Ceramic Society 72(5) (1989) 725-734.
[83] F.F. Lange, B.J. Kellett, Thermodynamics of densification .2. Grain growth in porous compacts and relation to densification, Journal of the American Ceramic Society 72(5) (1989) 735-741.
[84] F.F. Lange, Densification of powder compacts: An unfinished story, Journal of the European Ceramic Society 28(7) (2008) 1509-1516.
[85] R.H.R. Castro, Controlling sintering and grain growth of nanoceramics, Cerâmica 65 (2019) 122-129.
[86] H. Li, F.L. Souza, R.H.R. Castro, Kinetic and thermodynamic effects of manganese as a densification aid in yttria-stabilized zirconia, J. Eur. Ceram. Soc. 38(4) (2018) 1750-1759.